Final Report:

Magnetic Methods for the Identification of Aberrant (Incorrect) Microstructures in Grade 91 Steel

John W. Wilson and Anthony J. Peyton

Department of Electrical and Electronic Engineering,
School of Engineering,
Faculty of Science and Engineering,
University of Manchester,
Oxford Rd,
Manchester
M13 9PL

Date: 31st January 2020

EPRI Agreement: 10010570

1. Introduction

Ferromagnetic materials are made up of magnetic domains; regions in which the individual atomic magnetic dipoles are grouped together and aligned. When a magnetic field is applied to a ferromagnetic material, magnetic domains aligned close to the direction of magnetisation grow at the expense of other domains. As domain walls sweep through the material they interact with microstructural features such as grain boundaries, dislocations, cavities, precipitates, microcracks and impurity atoms and the movement of the domain walls is hindered or pinned by these features. Thus, through the application of a low frequency magnetic field, the magnetic properties of the material under inspection can be probed and relationships established between the magnetic response and the material microstructure. By comparing magnetic properties with microstructure or hardness, relationships can be established between specific magnetic signal features and microstructural changes, ultimately leading to a method for the assessment of incorrect microstructures in plant components.

The approach adopted by the University of Manchester (UoM) team is to combine three magnetic measurements to provide a holistic view of the magnetic response of the steel, as shown in Figure 1. The first, magnetic hysteresis, is achieved by plotting the flux density in the material (B) against the applied magnetic field (H). Various parameters can be extracted from the BH characteristics, including remanence and coercive field. The coercive field (Hc) is a measurement of magnetic hardness, which is often indicative of the material hardness and has also been shown to be related to dislocation density. As BH measurement is carried out at low excitation frequencies (<=1Hz), the measurement depth is greater than higher frequency magnetic / electromagnetic techniques such as eddy current, due to the electromagnetic skin effect. Thus, BH loop parameters can be said to be sensitive to both surface and bulk microstructural changes. As well as measurement of major BH loop, low amplitude perturbations (minor loops) can be superimposed on the low frequency BH loop and incremental permeability curves calculated from this. Minor loops have been shown to be more sensitive to lattice defects than the traditional structure-sensitive properties of the major loop. The third proposed inspection technique is MBN; a high frequency signal superimposed on the major BH loop generated by discontinuous magnetic domain wall motion caused by domain wall pinning. Through analysis of the MBN signal, information pertaining to lattice defects such as dislocations, grain boundaries, impurity atoms and precipitates can be gathered. However, as MBN is a high frequency phenomenon, its measurement depth is limited.

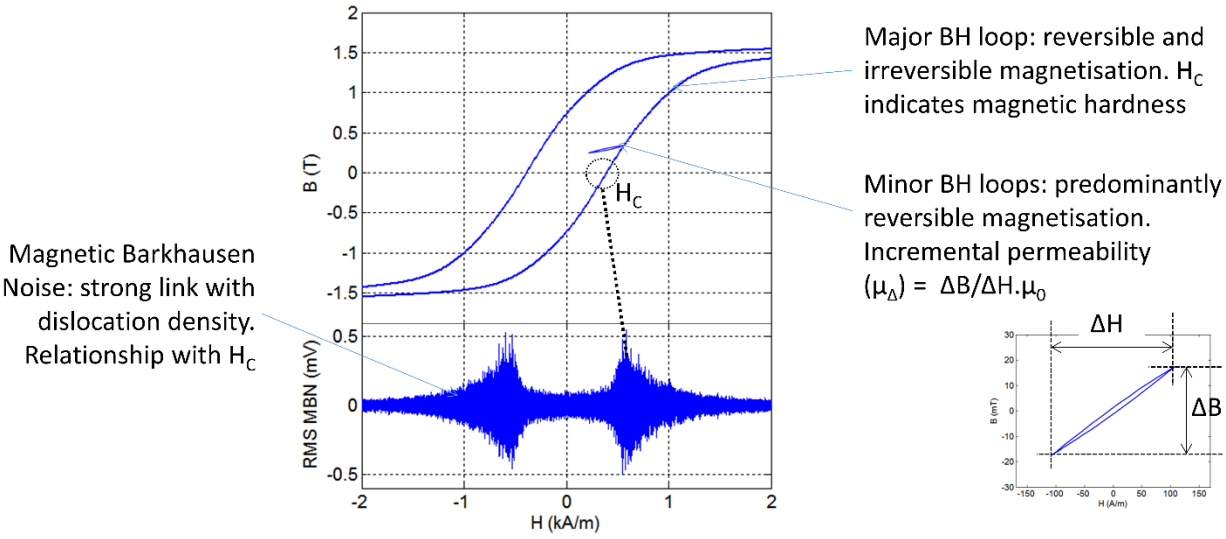

Figure 1. Measured magnetic parameters

2. Technique Description

Figure 2 shows the current generation of magnetic inspection tool. The tool features a replaceable excitation core to allow the user to match the pole faces to the geometry of the component under inspection ensuring efficient magnetic coupling and a sprung sensor head to ensure close proximity of the sensors to the material under inspection. The version of the probe shown here is constructed

in a Perspex box to allow the inner components to be seen for demonstration purposes. A version of the tool in a ruggedised enclosure for field deployment has also been developed along with a portable, battery powered control box.

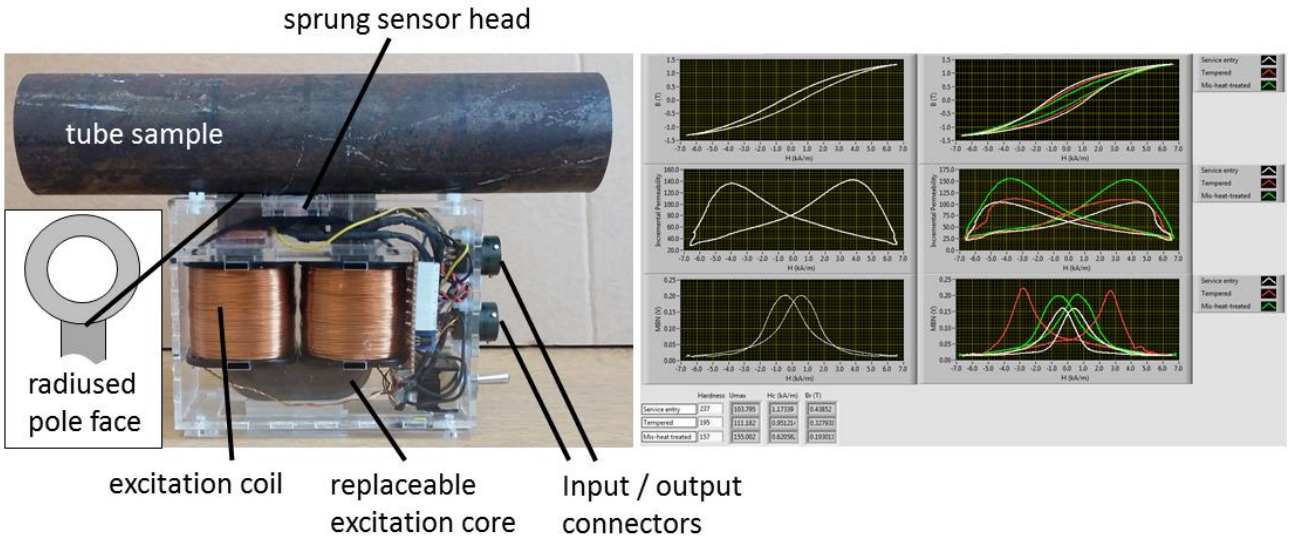

Figure 2. Current generation of EM measurement tool

Table 1 provides a comparison of the techniques employed in this work. The coercive field, derived from the major BH loop, provides a measurement of magnetic hardness which is often indicative of material hardness. As a low frequency / high amplitude signal is required, it has the greatest penetration depth of the techniques described here but it does require a relatively long measurement time in the order of tens of seconds. Incremental permeability, derived from minor BH loops, utilises higher frequency excitation so measurement time is reduced, as is measurement depth. Both coercive field and incremental permeability are sensitive to sample thickness (<≈10 mm for Grade 91 steel). As MBN is directly generated by the interaction of magnetic domains with the material microstructure it can potentially provide a wealth of information about the material under inspection, the signal is however attenuated as it propagates through the material so measurement depth is limited (< 1mm) and it can be very sensitive to surface conditions.

Table 1. Advantages and disadvantages of inspection techniques

	Advantages	**Disadvantages**
Coercive field	Measures magnetic hardness – direct link to mechanical hardness No surface preparation needed	Low frequency (0.1Hz - 1Hz) so long measurement time Sensitive to material thickness if <≈10mm
Incremental permeability	Higher excitation frequency (10Hz) so shorter measurement time Lower amplitude = lower power so potentially lighter/less bulky equipment No surface preparation needed	Sensitive to material thickness if <≈10mm
MBN	Signal has direct link to material microstructure	Low frequency (0.1Hz - 1Hz) so long measurement time Low measurement depth (<1mm) so sensitive to surface conditions

3. Sample Preparation

The samples were not exposed to mechanical loading, heating, cutting or machining. No surface preparation was carried out. The sections of pipe sections provided for testing all had areas where the surface had been subjected to grinding. As all the inspection techniques employed here have some degree of sensitivity to surface conditions, it was decided that two sets of measurements would be collected on each sample; one set of nine measurements from the ground area and one set of nine measurements from the unground area.

Figure 3 and Figure 4 show a schematic and photograph respectively of the two areas. Because of the pattern of the grinding (see Figure 4) and resultant accessibility for the probe, measurements were taken in slightly different positions for some of the samples. For the ground areas, some samples had measurements taken in positions A, B and D whereas others had measurements taken in positions A, C and D; see Table 4 to Table 9. Measurement positions for the unground areas were the same for all samples.

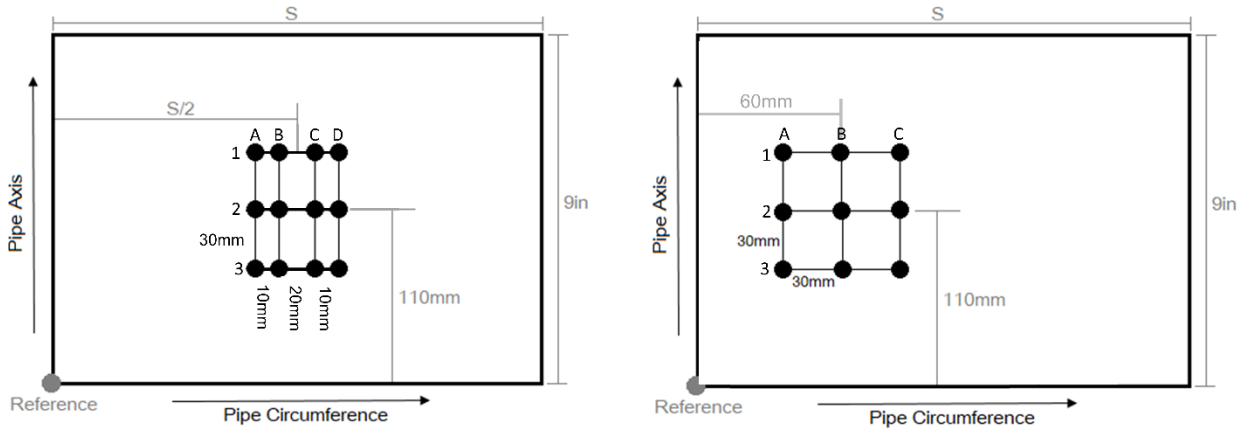

Scan positions for 'ground' measurements

Scan positions for 'unground' measurements

Figure 3. Schematic of measurement positions for pipe samples

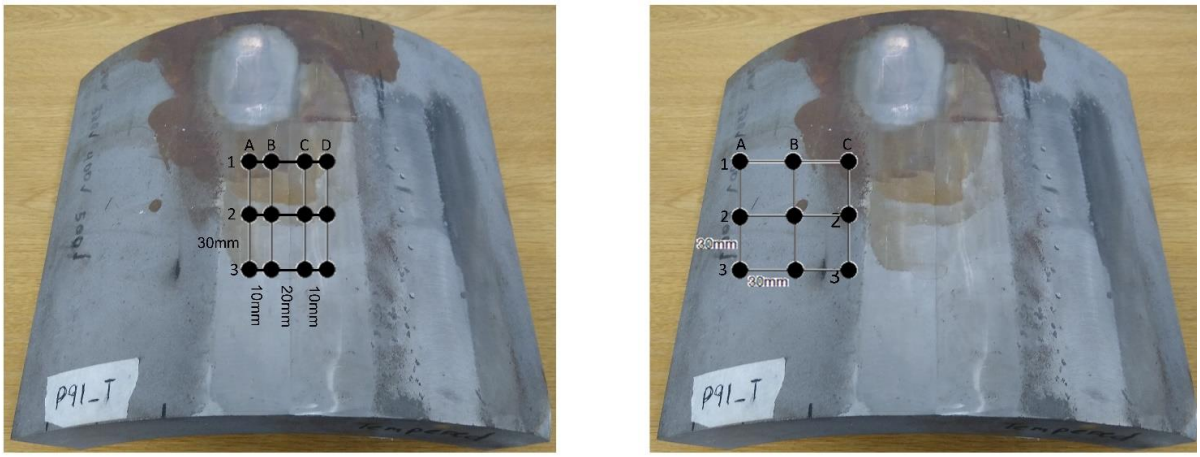

Scan positions for 'ground' measurements

Scan positions for 'unground' measurements

Figure 4. Photo of measurement positions for pipe samples

Figure 5 and Figure 6 show a diagram and photograph of the measurement positions for the tube samples. Measurements for each sample were taken in 30° increments in the centre of the sample. Radiused pole faces shaped to the geometry of the samples were used to ensure efficient magnetic coupling between sample and probe.

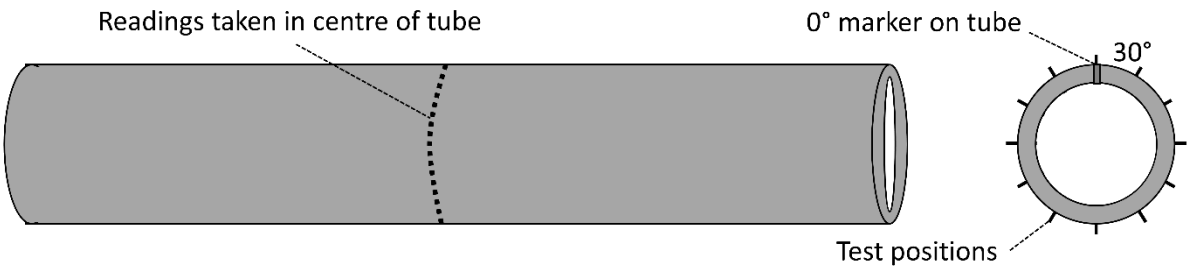

Figure 5. Measurement positions for tube samples

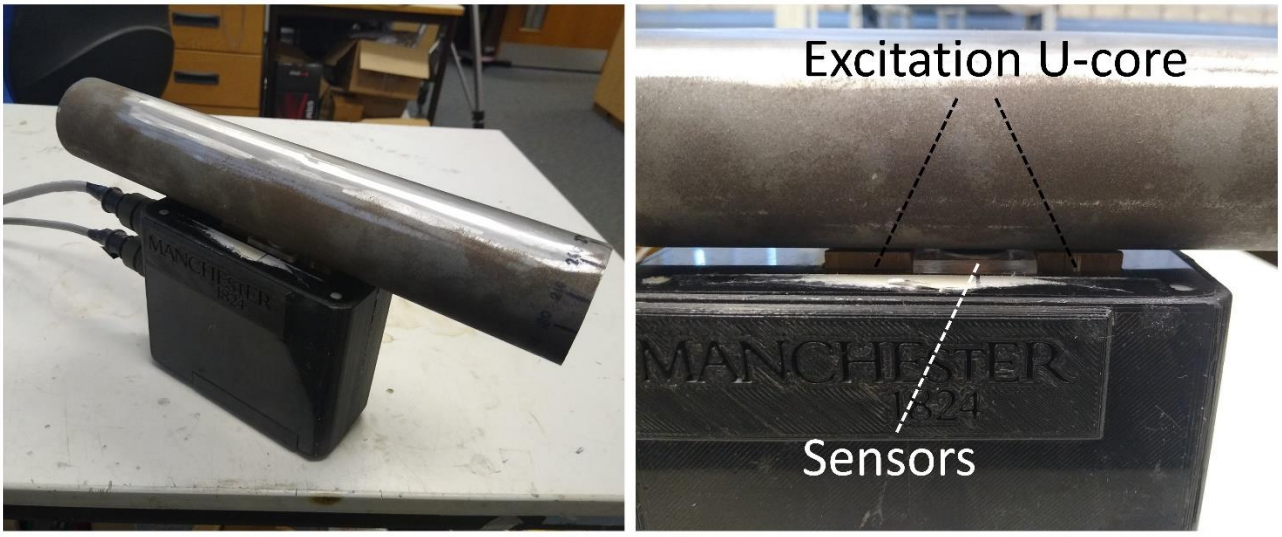

Figure 6. Photograph of test apparatus

Table 2 shows the short names used for the samples in this report; P91 for the pipe sections and T91 for the tube sections. Also shown is the actual median hardness supplied with the samples which is used as reference for the plots in the remainder of this report. It should be noted here that the hardness for tempered (P91_T and T91_T) and normalised and tempered (P91_N_T and T91_N_T) samples is very close and these measurements may not be clearly distinguished in the plots. Tables of all measurements have been provided in Appendix 1 to aid in the interpretation of the plots along with alternative plots of some data sets in Appendix 2.

Table 2. Sample short names and hardness reference

Condition	Pipe short name	Tube short name	Target Hardness (HV 5.0)	Actual Median Hardness
Fully Ferritic	**P91_FF**	**T91_FF**	160	**147**
HAZ + Tempered	**P91_HAZ_T**	**T91_HAZ_T**	215	**170**
Over-Tempered	**P91_OT**	**T91_OT**	185	**198**
Tempered	**P91_T**	**T91_T**	195	**207**
Normalized + Tempered	**P91_N_T**	**T91_N_T**	215	**208**
As received	**P91_AR**	**T91_AR**	215	**220**
HAZ	**P91_HAZ**	**T91_HAZ**	300	**405**
Normalized	**P91_N**	**T91_N**	425	**428**

4. Test Results from Pipe Samples

Figure 7 shows the coercive field derived from the major BH loop measurements for the unground (Figure 7a) and ground (Figure 7b) areas of the pipe sections. It can be seen from the plots that the increase in material hardness results in a corresponding increase in magnetic hardness as indicated by the increase in the coercive field. The fully ferritic (P91_FF), HAZ and tempered (P91_HAZ_T) and as received (P91_AR) samples can be clearly discriminated in both the ground and unground areas as can the harder HAZ (P91_HAZ) and normalized (P91_N) samples. However, the over-tempered (P91_OT), tempered (P91_T) and normalized and tempered (P91_N_T) are very close in terms of both the magnetic measurements and hardness.

Comparison of the measurements from the unground (Figure 7a) and ground (Figure 7b) areas show that grinding does have some impact, resulting in lower readings in the ground area for some of the samples. It should be noted that the impact of grinding on the readings is greater for the harder P91_T and P91_N_T samples and P91_AR and P91_FF could still be easily separated even if readings were taken in areas with different surface conditions. Source data is shown in Appendix 1 (Table 4 and Table 5) and alternate plots excluding the hardest two samples for clarity are shown in Appendix 2 (Figure 16).

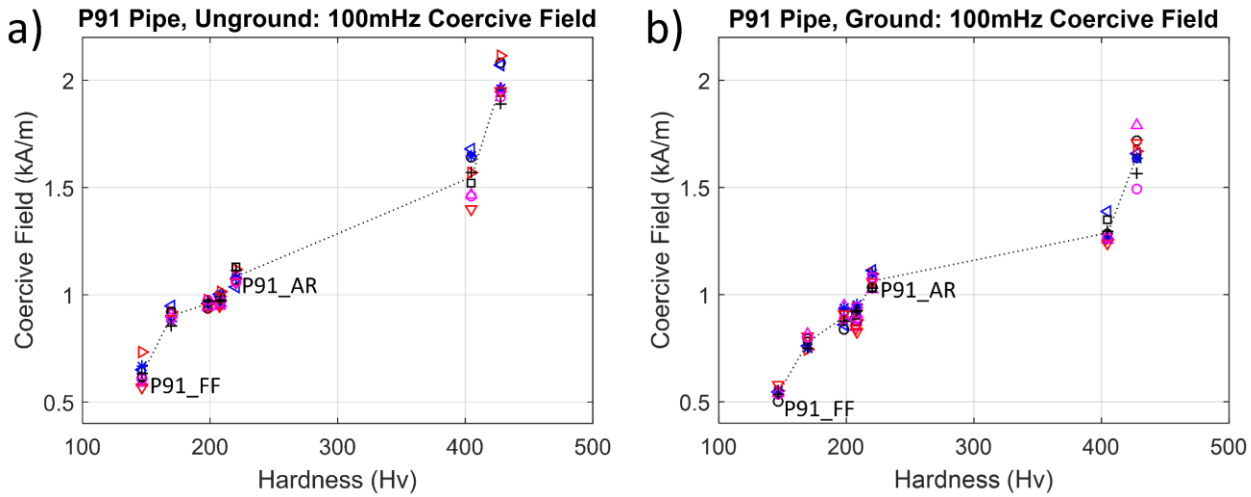

Figure 7. Plots of coercive field extracted from major loops measured on pipe sections; a) Measurements from unground area, b) Measurements from ground area

Figure 8 shows the incremental permeability derived from the minor loop measurements for the unground (Figure 8a) and ground (Figure 8b) areas of the pipe sections. The relationship between permeability and hardness is the inverse of the relationship between coercive field and hardness, with a decrease in permeability with increasing hardness and an overall higher level of permeability in the ground areas. The impact of surface conditions on permeability does seem to be greater than for the coercive field. This could be due to the higher frequency excitation employed for the permeability measurements resulting in a lower measurement depth and a greater sensitivity to surface conditions. Source data is shown in Appendix 1 (Table 6 and Table 7) and plots excluding the hardest two samples are shown in Appendix 2 (Figure 17).

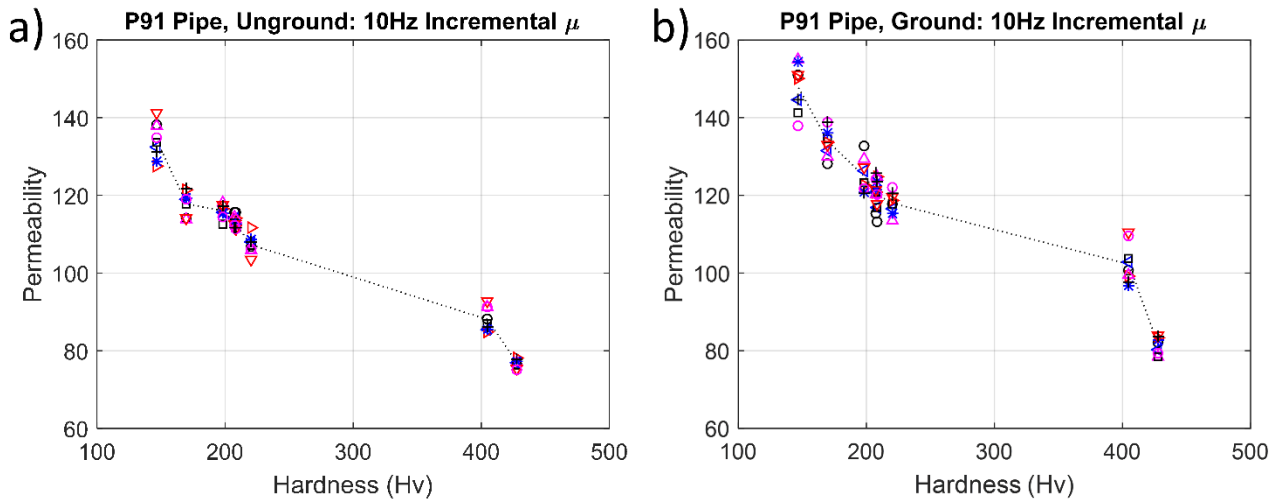

Figure 8. Plots of incremental permeability extracted from minor loops measured on pipe sections; a) Measurements from unground area, b) Measurements from ground area

Figure 9 shows the peak amplitude derived from the MBN profiles for the pipe samples. The results for the unground area of the pipe section (Figure 9a) do appear to show some correlation with hardness if the results for the harder two samples are disregarded. However, there is a great deal of scatter in the results for the ground area of the pipe section (Figure 9b), probably due to the sensitivity of MBN to surface conditions.

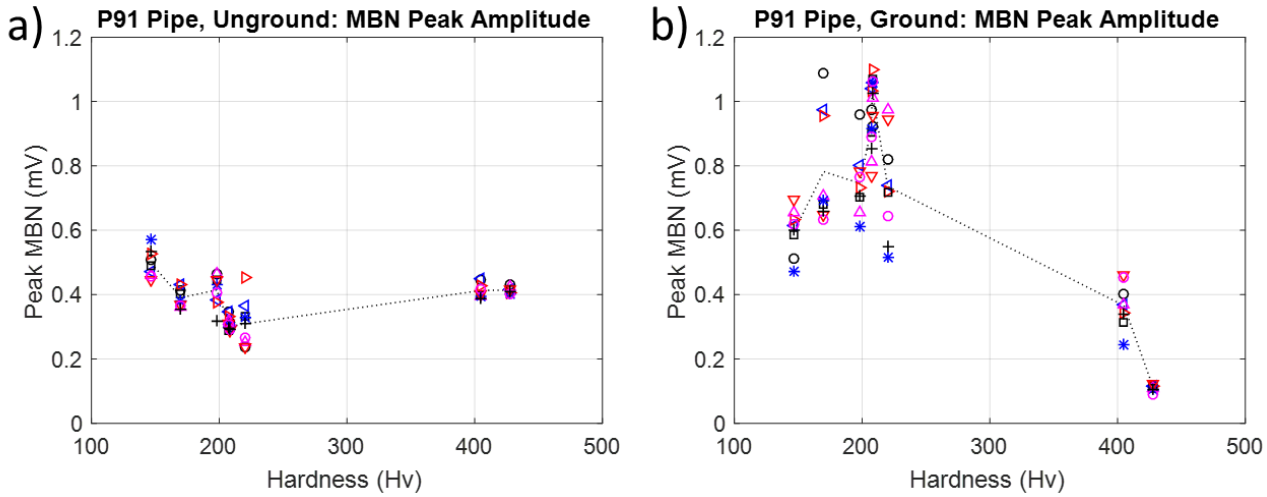

Figure 9. Plots of MBN peak amplitude extracted from MBN profiles measured on pipe sections; a) Measurements from unground area, b) Measurements from ground area

5. Test Results from Tube Samples

5.1. Identified Tube Samples (Tube Set A)

Figure 10a shows the coercive field derived from the major BH loop measurements for the identified tube samples (tube set A). It can be seen from the plots that, like the pipe samples, the coercive field increases for increasing hardness. However, some geometrical effects are evident from the results, as the wall thickness is much smaller than the pipe. Firstly, the maximum coercive field for the tube samples is much greater than for the pipe samples. Secondly, the coercive field polar plot for T91_OT (Figure 10b) is asymmetric in comparison to the polar plots for the other tubes samples; for example T91_N shown in Figure 10c. The most likely explanation for this is a variation in wall thickness skewing the magnetic measurements. An alternate explanation is uneven heat treatment during tube manufacture, though this would be detected through hardness measurements.

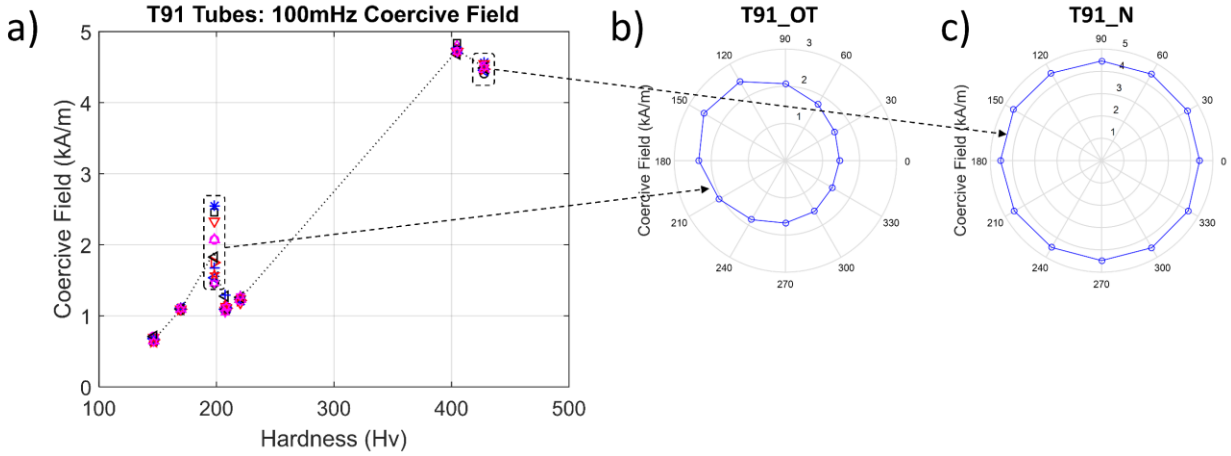

Figure 10. a) Plot of coercive field extracted from major loops measured on tube set A, b) Polar plot of coercive field from T91_OT, b) Polar plot of coercive field from T91_N

Figure 11a shows the incremental permeability derived from the minor loop measurements for the identified tube samples. Like the pipe samples, the relationship between permeability and hardness is the inverse of the relationship between coercive field and hardness. Some asymmetry is also evident in the polar plot for T91_OT (Figure 11b). However, the asymmetry is not as great as for the coercive field possibly because of the lower measurement depth for incremental permeability.

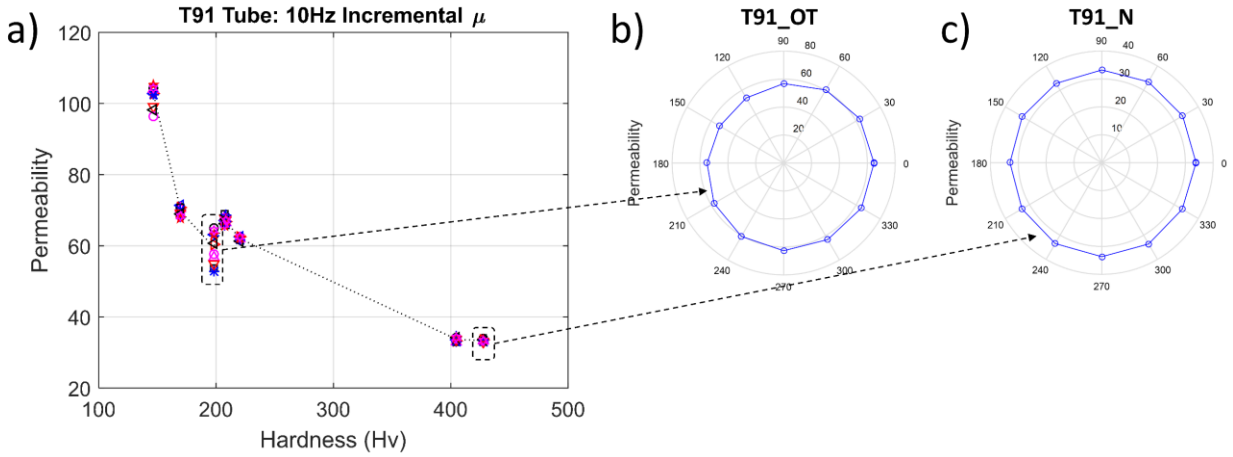

Figure 11. Plot of incremental permeability extracted from minor loops measured on tube set A, b) Polar plot of incremental permeability from T91_OT, b) Polar plot of incremental permeability from T91_N

Figure 12 shows the peak amplitude derived from the MBN profiles for the tube samples. As with the plot for the tube samples (Figure 9) there is a great deal of scatter, especially for the softer samples. No reliable correlation to hardness can be drawn from the MBN data.

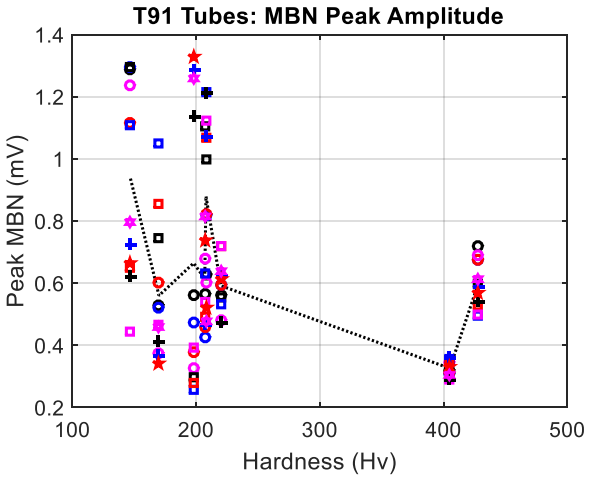

Figure 12. Plot of MBN peak amplitude measured on tube set A

5.2. Unidentified Tube Samples (Tube Set B)

A full set of measurements were carried out on the unidentified tube set B. Results for the identified and unidentified tubes are tabulated in Appendix 1 and a full set of polar plots for both sets of tubes are provided in Appendix 2. Using this data, identification of the tubes was attempted and is shown in Table 3. The values for the columns in grey are very close and identification is not certain. It should be noted that the wall thickness of these samples makes identification difficult and any it is possible that geometric effects have dominated these results.

Table 3. Average coercive field and incremental permeability values from identified (set A) and unidentified (set B) tube samples. Columns for 'B' samples represent best guess for sample identification. Grey columns too close to identify with confidence

	Samples							
	T91_FF	**T91_HAZ_T**	**T91_OT**	**T91_T**	**T91_N_T**	**T91_AR**	**T91_HAZ**	**T91_N**
Coercive Field (kA/m)	0.671	1.098	1.810	1.131	1.110	1.237	4.739	4.495
Incremental Permeability	102.18	69.58	59.60	67.05	67.21	62.04	33.68	33.33
	B7	**B1**	**B8**	**B3**	**B2**	**B5**	**B6**	**B4**
Coercive Field (kA/m)	0.676	1.099	2.062	1.079	1.1052	1.432	4.700	4.508
Incremental Permeability	100.48	68.40	57.55	66.47	68.47	65.12	34.01	32.97

Figure 13a shows a plot of the coercive field for the unidentified tube set B plotted with respect to hardness as labelled in Table 3. The plot for the identified tube set A is also shown in Figure 13b for

comparison. It can be seen from the plots that the two sets of data are largely comparable, with the asymmetric T91_OT corresponding to sample B8. It is possible that these two samples are from the same **tube** but have <u>not</u> undergone the same **heat treatment**, i.e. the samples may have been identified by their geometry rather than by their heat treatment. Source data is shown in Appendix 1 (Table 10 and Table 14) and alternate plots excluding the hardest two samples are shown in Appendix 2 (Figure 18).

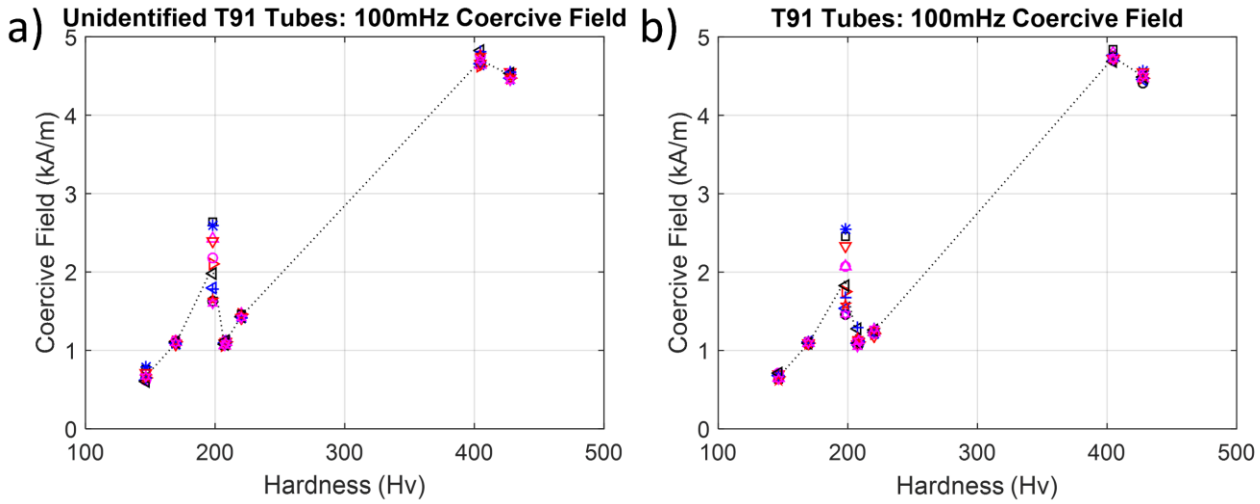

Figure 13. Plot of coercive field extracted from major loops measured on tube sections; a) Unidentified 'B' tubes as labelled in Table 3, b) Identified 'A' tubes

Figure 14 shows incremental permeability and for the identified and unidentified tube samples. As for the coercive field there is a good match between the two plots. Absolute values are lower than for the pipe samples due to the low wall thickness. Source data is shown in Appendix 1 (Table 11 and Table 14) and alternate plots excluding the hardest two samples are shown in Appendix 2 (Figure 19).

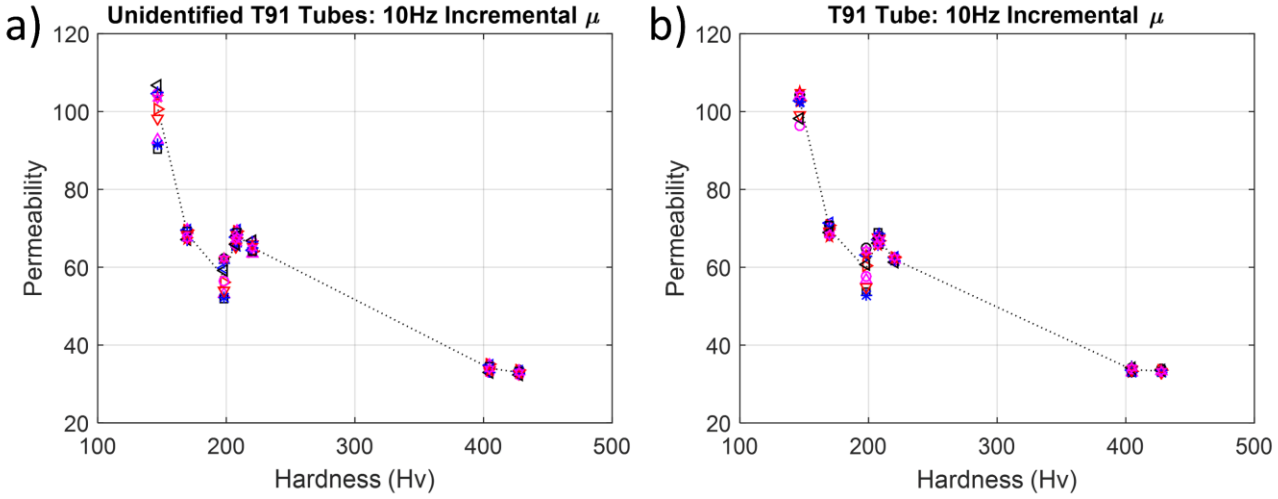

Figure 14. Plot of incremental permeability extracted from minor loops measured on tube sections; a) Unidentified 'B' tubes as labelled in Table 3, b) Identified 'A' tubes

Figure 15 shows the peak MBN measurements for the tube samples. Although there does not appear to be any direct correlation with hardness, the overall trend of the data does appear to be similar. The greater scatter in the plot for the identified tubes (Figure 15b) is due to surface conditions; the 'B' set of tubes were mostly untouched, whereas the 'A' set had large areas of surface grinding.

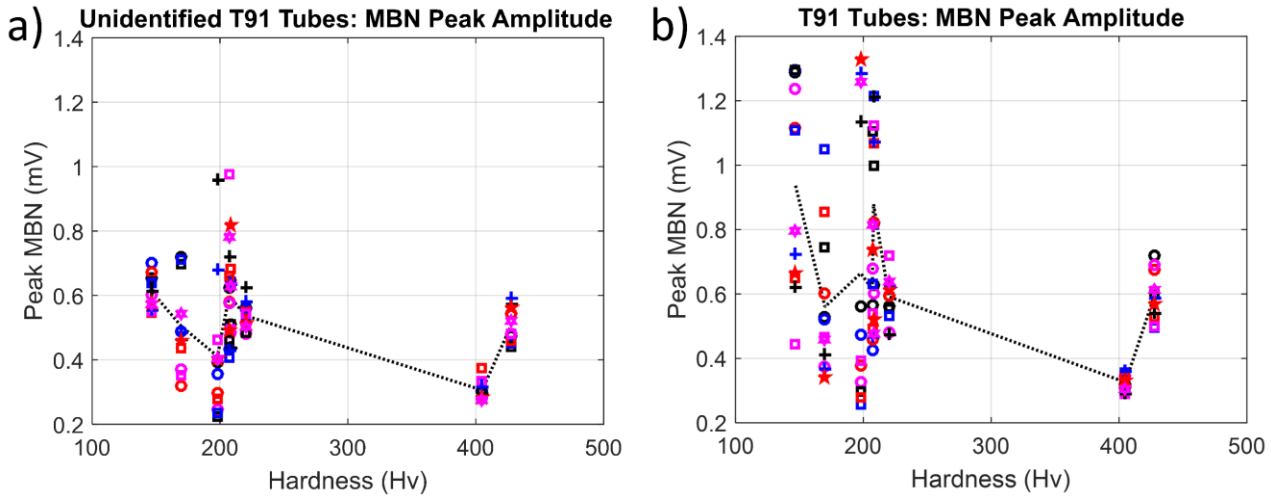

Figure 15. Plots of MBN peak amplitude extracted from MBN profiles measured on tubes; a) Unidentified 'B' tubes as labelled in Table 3, b) Identified 'A' tubes

6. Discussion and Conclusions

The results from the pipe sections show that there is a strong correlation between both coercive field and incremental permeability and hardness for the sample set used in these tests. Tests were carried out on areas with and without surface preparation (grinding) and although there is some change in the overall amplitude between the ground and unground areas this change is small, especially if the two samples with hardness >400 Hv are disregarded. This indicates that for industrial deployment, surface conditions can, to some extent, be disregarded. Three pipe samples with very close hardness values were included in these tests: P91_OT (198 Hv), P91_T (207 Hv) and P91_N_T (208 Hv). Using this technique, it would not be possible to discriminate between these three samples due to their almost identical magnetic response. MBN shows an overall decrease in amplitude for increasing hardness (<400 Hv) for the unground areas on the samples but this correlation is lost for the measurements on the ground areas due to surface conditions.

The coercive field and incremental permeability measurements on the set A (identified) tube samples follow the same trends as the pipe section samples with an increase in coercive field and decrease in incremental permeability for increasing hardness. A full set of magnetic measurements was made on tube set B and an attempt was made to identify the tubes with reference to these measurements. The results of this are shown in Table 3, though identification of three of the samples (T91_HAZ_T, T91_T and T91_N_T) is uncertain.

Interpretation of the results for the tube samples and identification of the samples in tube set B is complicated by the thin walls of the tubes. At wall thickness <≈10mm, the geometry of the tube has a strong influence on the magnetic measurements. It may be possible to mitigate this by utilising accurate wall thickness measurement, using ultrasonic testing for example, to correct the magnetic measurements but this has not been attempted in this study.

The work detailed in this report shows that magnetic measurements have great potential for microstructural assessment of Grade 91 steel, especially for the identification of incorrect (aberrant) microstructures. Tests show that although surface conditions do cause variations in coercive field and incremental permeability measurements, the effect is small enough to manage, though sensitivity to surface conditions does seem to rule out MBN for this application. Variations in component thickness have more of an impact on the measurement techniques used here though previous tests show that this should not be a problem if the component thickness is <≈10mm. For thinner samples it may be possible to correct for material thickness if accurate thickness measurements can be obtained.

Appendix 1: Tables of Test Values

Table 4. Coercive field (kA/m) for ground areas on pipe samples

	Measurement position											
Sample	**A1**	**A2**	**A3**	**B1**	**B2**	**B3**	**C1**	**C2**	**C3**	**D1**	**D2**	**D3**
P91_FF	0.503	0.547	0.553	0.542	0.540	0.549				0.577	0.535	0.537
P91_HAZ_T	0.794	0.762	0.743	0.813	0.784	0.752				0.804	0.801	0.750
P91_OT	0.839	0.860	0.885				0.948	0.918	0.938	0.910	0.889	0.876
P91_T	0.879	0.926	0.938				0.848	0.904	0.935	0.846	0.889	0.921
P91_N_T	0.879	0.885	0.884	0.912	0.934	0.956				0.824	0.940	0.926
P91_AR	1.035	1.111	1.097	1.024	1.031	1.099				1.060	1.080	1.030
P91_HAZ	1.281	1.388	1.258	1.255	1.351	1.260				1.238	1.267	1.294
P91_N	1.717	1.657	1.669	1.791	1.634	1.636				1.707	1.492	1.564

Table 5. Coercive field (kA/m) for unground areas on pipe samples

	Measurement position								
	A1	**A2**	**A3**	**B1**	**B2**	**B3**	**C1**	**C2**	**C3**
P91_FF	0.611	0.648	0.736	0.589	0.616	0.668	0.570	0.604	0.631
P91_HAZ_T	0.918	0.950	0.922	0.907	0.921	0.875	0.889	0.891	0.856
P91_OT	0.937	0.957	0.974	0.942	0.957	0.955	0.944	0.973	0.971
P91_T	0.961	1.003	0.989	0.946	0.968	0.963	0.946	0.964	0.972
P91_N_T	0.990	0.989	1.016	0.957	0.977	0.972	0.959	0.970	0.976
P91_AR	1.066	1.035	1.120	1.092	1.129	1.082	1.059	1.055	1.114
P91_HAZ	1.639	1.678	1.572	1.463	1.522	1.645	1.397	1.457	1.568
P91_N	2.081	2.071	2.114	1.959	1.942	1.960	1.949	1.922	1.891

Table 6. Incremental permeability values for ground areas on pipe samples

	Measurement position											
Sample	**A1**	**A2**	**A3**	**B1**	**B2**	**B3**	**C1**	**C2**	**C3**	**D1**	**D2**	**D3**
P91_FF	151.1	144.7	150.0	154.8	141.2	154.3				150.9	137.8	144.6
P91_HAZ_T	128.2	131.5	133.6	129.9	134.6	136.1				133.0	139.0	139.0
P91_OT	132.9	126.3	122.8				129.5	123.4	120.8	127.1	121.8	120.7
P91_T	115.5	120.8	120.7				120.3	120.8	121.3	121.5	124.1	125.8
P91_N_T	113.3	116.9	124.8	124.9	116.9	123.6				117.9	120.2	123.6
P91_AR	117.8	116.4	118.8	113.6	117.8	115.3				119.7	122.1	120.5
P91_HAZ	100.7	102.8	99.1	99.4	103.7	96.7				110.6	109.5	97.7
P91_N	82.1	80.3	83.3	78.5	78.3	82.9				83.8	79.5	83.6

Table 7. Incremental permeability values for unground areas on pipe samples

	Measurement position								
	A1	**A2**	**A3**	**B1**	**B2**	**B3**	**C1**	**C2**	**C3**
P91_FF	138.3	132.3	127.4	138.0	133.6	128.6	141.2	134.8	131.3
P91_HAZ_T	114.2	119.1	121.4	113.7	117.7	119.2	114.2	119.1	121.8
P91_OT	117.3	115.8	116.5	118.2	112.5	115.5	117.5	114.5	117.1
P91_T	115.7	114.2	113.5	114.5	112.8	112.3	112.7	112.1	111.7
P91_N_T	115.7	113.3	114.1	113.9	111.8	112.4	111.2	111.3	111.5
P91_AR	106.8	108.2	111.6	105.8	107.0	108.6	103.4	106.1	108.1
P91_HAZ	88.2	85.5	84.8	91.3	86.9	85.6	92.9	91.1	86.1
P91_N	76.7	76.9	78.1	77.0	76.2	77.1	75.5	75.1	77.7

Table 8. Peak MBN (mV) for ground areas on pipe samples

Sample	Measurement position											
	A1	A2	A3	B1	B2	B3	C1	C2	C3	D1	D2	D3
P91_FF	0.510	0.616	0.634	0.657	0.585	0.472				0.696	0.618	0.602
P91_HAZ_T	1.086	0.975	0.957	0.705	0.682	0.690				0.649	0.635	0.660
P91_OT	0.958	0.803	0.733				0.654	0.702	0.611	0.783	0.766	0.706
P91_T	0.973	1.040	1.032				0.813	0.904	0.915	0.770	0.891	0.852
P91_N_T	0.922	1.059	1.100	1.012	1.071	1.060				0.957	1.064	1.027
P91_AR	0.821	0.740	0.721	0.975	0.719	0.515				0.944	0.643	0.548
P91_HAZ	0.402	0.369	0.343	0.370	0.314	0.243				0.461	0.452	0.338
P91_N	0.115	0.115	0.116	0.108	0.109	0.106				0.122	0.091	0.103

Table 9. Peak MBN (mV) for unground areas on pipe samples

	Measurement position								
	A1	A2	A3	B1	B2	B3	C1	C2	C3
P91_FF	0.507	0.473	0.528	0.461	0.490	0.572	0.446	0.459	0.533
P91_HAZ_T	0.413	0.432	0.432	0.363	0.402	0.382	0.370	0.367	0.354
P91_OT	0.463	0.384	0.376	0.464	0.446	0.430	0.447	0.404	0.318
P91_T	0.348	0.345	0.334	0.318	0.288	0.305	0.309	0.308	0.295
P91_N_T	0.314	0.300	0.301	0.314	0.305	0.301	0.288	0.290	0.293
P91_AR	0.237	0.366	0.453	0.252	0.332	0.328	0.236	0.267	0.311
P91_HAZ	0.446	0.449	0.427	0.394	0.399	0.395	0.401	0.416	0.388
P91_N	0.430	0.415	0.404	0.426	0.418	0.403	0.417	0.402	0.411

Table 10. Coercive field (kA/m) for identified tube samples

Sample	Measurement position											
	0°	30°	60°	90°	120°	150°	180°	210°	240°	270°	300°	330°
P91_FF	0.678	0.681	0.668	0.647	0.633	0.678	0.699	0.718	0.719	0.659	0.626	0.641
P91_HAZ_T	1.080	1.107	1.093	1.096	1.113	1.111	1.093	1.108	1.098	1.092	1.088	1.094
P91_OT	1.459	1.542	1.751	2.070	2.452	2.542	2.337	2.067	1.833	1.678	1.576	1.455
P91_T	1.074	1.100	1.101	1.112	1.112	1.091	1.071	1.131	1.279	1.296	1.155	1.051
P91_N_T	1.079	1.091	1.102	1.139	1.117	1.108	1.106	1.123	1.100	1.118	1.118	1.117
P91_AR	1.244	1.228	1.220	1.223	1.243	1.210	1.186	1.222	1.259	1.273	1.266	1.270
P91_HAZ	4.707	4.763	4.769	4.799	4.836	4.734	4.714	4.722	4.692	4.705	4.714	4.711
P91_N	4.405	4.460	4.476	4.466	4.525	4.559	4.546	4.525	4.493	4.479	4.509	4.499

Table 11. Incremental permeability for identified tube samples

Sample	Measurement position											
	0°	30°	60°	90°	120°	150°	180°	210°	240°	270°	300°	330°
P91_FF	104.3	102.8	102.8	103.9	104.4	102.5	99.0	96.4	98.1	102.4	105.2	104.3
P91_HAZ_T	70.7	71.3	70.7	70.6	70.8	70.2	69.4	68.4	68.9	68.2	67.6	68.3
P91_OT	64.8	63.1	60.3	56.8	53.7	52.9	54.9	57.7	60.6	62.7	63.2	64.4
P91_T	66.9	67.3	66.8	68.0	69.0	68.1	67.6	67.6	66.3	65.7	65.5	66.0
P91_N_T	68.1	67.0	66.9	66.4	65.9	66.7	67.4	67.8	67.4	68.6	67.5	67.0
P91_AR	62.6	62.5	62.6	61.9	61.7	61.7	61.8	61.8	61.4	61.6	62.1	62.7
P91_HAZ	34.1	33.7	33.2	32.9	33.0	33.0	33.6	33.9	34.3	34.3	34.2	34.1
P91_N	33.8	33.5	33.5	33.2	32.8	33.0	33.0	33.1	33.5	33.7	33.6	33.3

Table 12. Peak MBN (mV) for identified tube samples

Sample	Measurement position											
	0°	30°	60°	90°	120°	150°	180°	210°	240°	270°	300°	330°
P91_FF	1.287	1.297	1.114	1.238	1.296	1.107	0.649	0.445	0.619	0.724	0.665	0.798
P91_HAZ_T	0.528	0.522	0.603	0.375	0.743	1.051	0.857	0.467	0.410	0.367	0.342	0.457
P91_OT	0.562	0.473	0.378	0.326	0.297	0.259	0.277	0.394	1.135	1.284	1.327	1.260
P91_T	0.564	0.426	0.460	0.677	1.104	0.632	0.493	0.541	0.464	0.467	0.738	0.814
P91_N_T	0.627	0.819	0.822	0.602	0.998	1.216	1.068	1.124	1.212	1.072	0.520	0.476
P91_AR	0.562	0.594	0.594	0.482	0.554	0.532	0.718	0.721	0.472	0.623	0.613	0.638
P91_HAZ	0.318	0.307	0.311	0.346	0.352	0.356	0.349	0.289	0.291	0.361	0.330	0.303
P91_N	0.720	0.674	0.676	0.691	0.597	0.496	0.527	0.499	0.541	0.586	0.569	0.612

Table 13. Coercive field (kA/m) for unidentified tube samples

	Measurement position											
Sample	**0°**	**30°**	**60°**	**90°**	**120°**	**150°**	**180°**	**210°**	**240°**	**270°**	**300°**	**330°**
B1	1.092	1.093	1.113	1.106	1.092	1.076	1.085	1.121	1.114	1.100	1.107	1.100
B2	1.077	1.105	1.110	1.116	1.113	1.111	1.109	1.131	1.129	1.093	1.079	1.090
B3	1.074	1.087	1.062	1.058	1.062	1.099	1.100	1.079	1.080	1.102	1.086	1.064
B4	4.494	4.480	4.472	4.516	4.512	4.520	4.548	4.534	4.531	4.548	4.492	4.446
B5	1.424	1.433	1.458	1.453	1.454	1.413	1.411	1.425	1.437	1.412	1.442	1.421
B6	4.652	4.649	4.625	4.635	4.669	4.675	4.658	4.758	4.820	4.802	4.761	4.699
B7	0.651	0.621	0.653	0.734	0.762	0.782	0.707	0.620	0.607	0.647	0.663	0.671
B8	1.622	1.803	2.107	2.416	2.630	2.586	2.398	2.184	1.973	1.784	1.642	1.593

Table 14. Incremental permeability for unidentified tube samples

	Measurement position											
Sample	**0°**	**30°**	**60°**	**90°**	**120°**	**150°**	**180°**	**210°**	**240°**	**270°**	**300°**	**330°**
B1	69.4	69.6	69.6	69.7	69.2	68.8	68.2	67.6	67.1	66.8	67.2	67.5
B2	68.0	67.8	67.3	66.4	65.5	65.2	65.2	65.7	66.0	66.5	67.1	67.0
B3	69.4	69.5	69.3	69.3	68.9	68.4	68.4	68.1	67.9	67.5	67.3	67.7
B4	33.5	33.4	33.6	33.4	33.2	32.8	32.6	32.4	32.4	32.5	32.7	33.0
B5	64.3	64.3	64.0	63.6	63.9	64.9	65.8	66.6	66.9	66.5	65.7	65.0
B6	34.9	34.9	35.2	34.9	34.6	34.2	33.6	33.1	32.8	32.8	33.3	33.9
B7	104.7	104.5	100.6	92.7	90.2	91.4	98.2	104.7	106.7	104.8	103.8	103.3
B8	62.3	59.7	56.2	53.2	51.8	52.3	54.1	56.6	59.0	60.9	62.2	62.4

Table 15. Peak MBN (mV) for unidentified tube samples

	Measurement position											
Sample	**0°**	**30°**	**60°**	**90°**	**120°**	**150°**	**180°**	**210°**	**240°**	**270°**	**300°**	**330°**
B1	0.717	0.490	0.320	0.370	0.697	0.712	0.435	0.351	0.461	0.485	0.459	0.543
B2	0.509	0.648	0.646	0.484	0.510	0.644	0.681	0.495	0.438	0.635	0.820	0.626
B3	0.623	0.433	0.579	0.574	0.462	0.408	0.660	0.977	0.718	0.430	0.493	0.782
B4	0.473	0.542	0.544	0.481	0.441	0.451	0.460	0.481	0.573	0.589	0.563	0.520
B5	0.561	0.558	0.514	0.480	0.484	0.532	0.550	0.544	0.623	0.581	0.515	0.503
B6	0.301	0.304	0.279	0.278	0.301	0.332	0.375	0.334	0.294	0.317	0.282	0.277
B7	0.652	0.702	0.672	0.602	0.643	0.640	0.546	0.550	0.613	0.553	0.577	0.573
B8	0.392	0.357	0.297	0.247	0.223	0.236	0.280	0.464	0.959	0.678	0.402	0.404

Appendix 2: Additional Figures

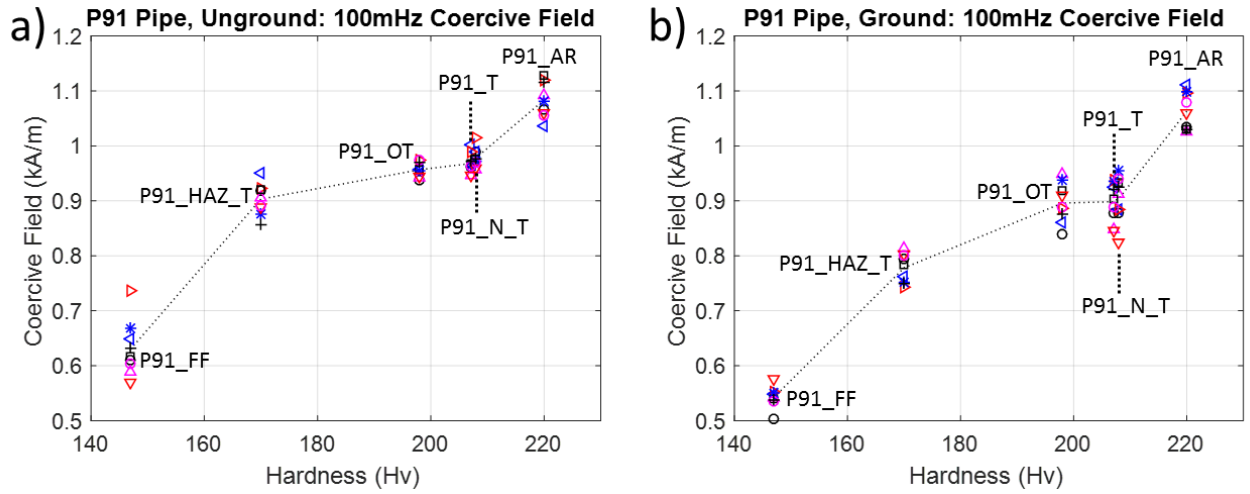

Figure 16. Plots of coercive field extracted from major loops measured on pipe sections; a) Measurements from unground area, b) Measurements from ground area. Excluding hardest two samples

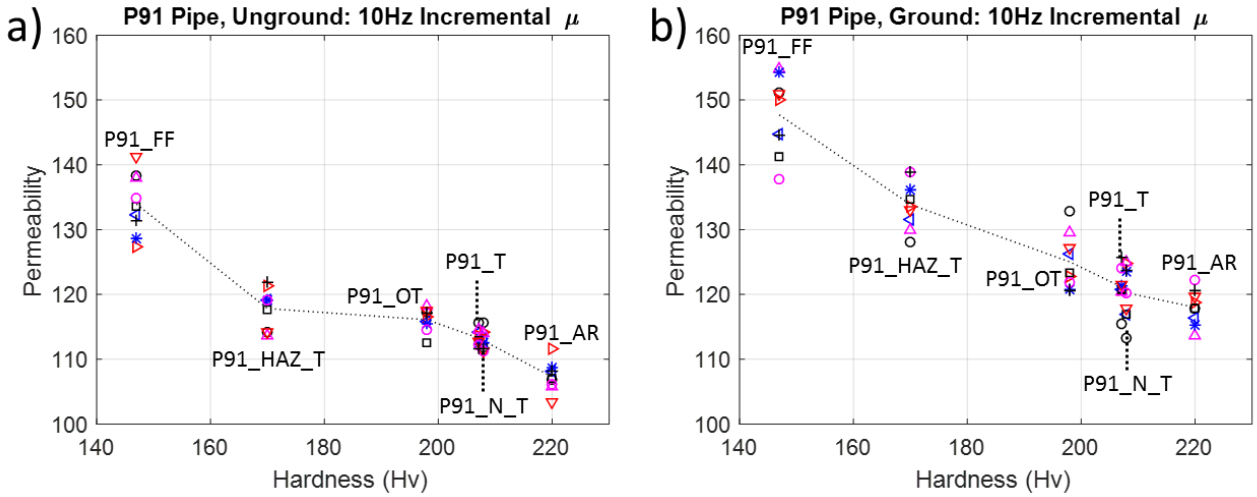

Figure 17. Plots of incremental permeability extracted from minor loops measured on pipe sections; a) Measurements from unground area, b) Measurements from ground area. Excluding hardest two samples

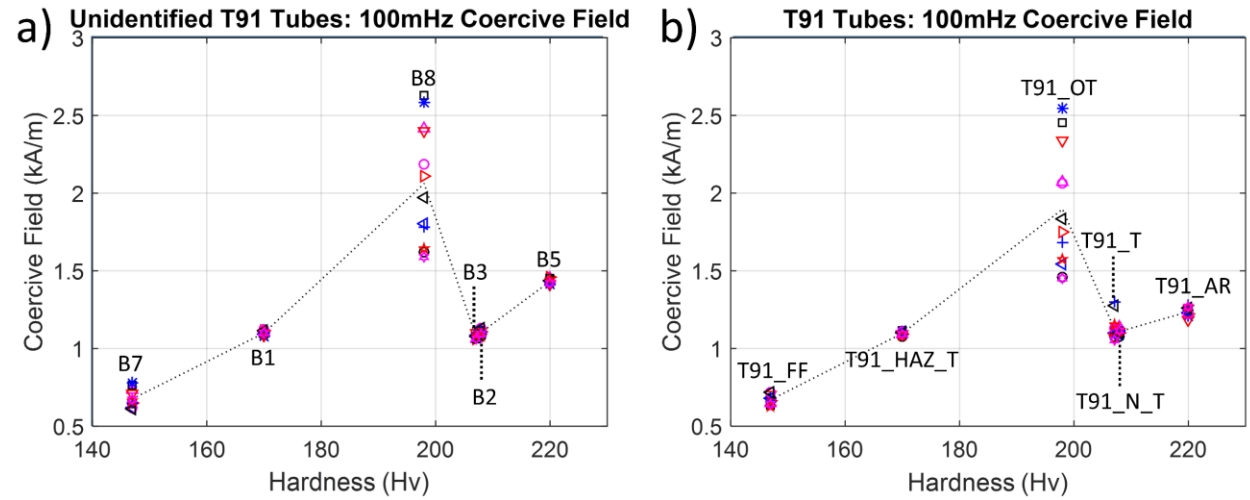

Figure 18. Plot of coercive field extracted from major loops measured on tube sections; a) Identified tubes, b) Unidentified 'B' tubes as labelled in Table 2. Excluding hardest two samples

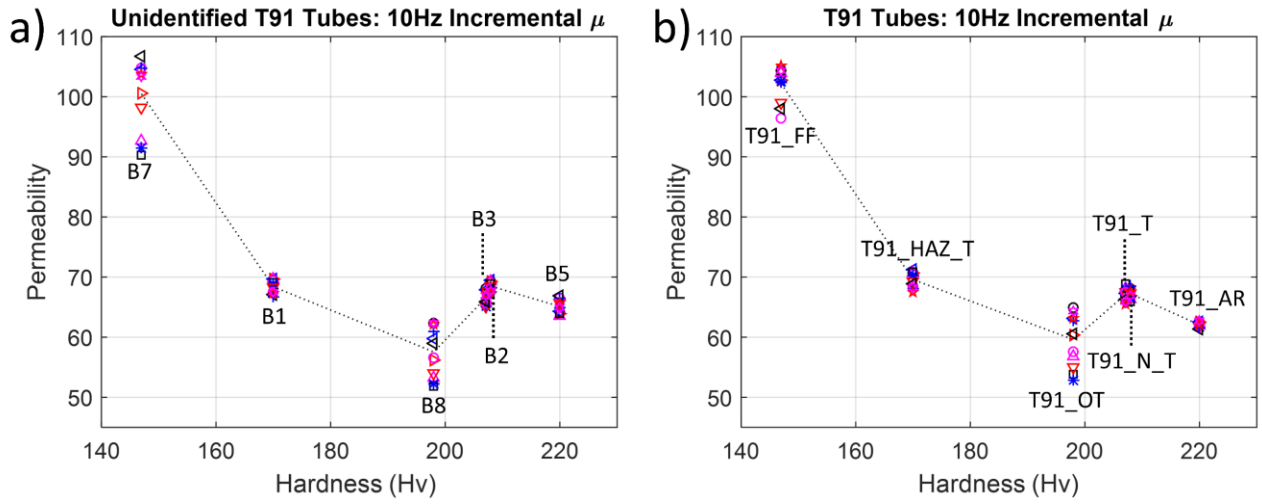

Figure 19. Plot of incremental permeability extracted from minor loops measured on tube sections; a) Identified tubes, b) Unidentified 'B' tubes as labelled in Table 2. Excluding hardest two samples

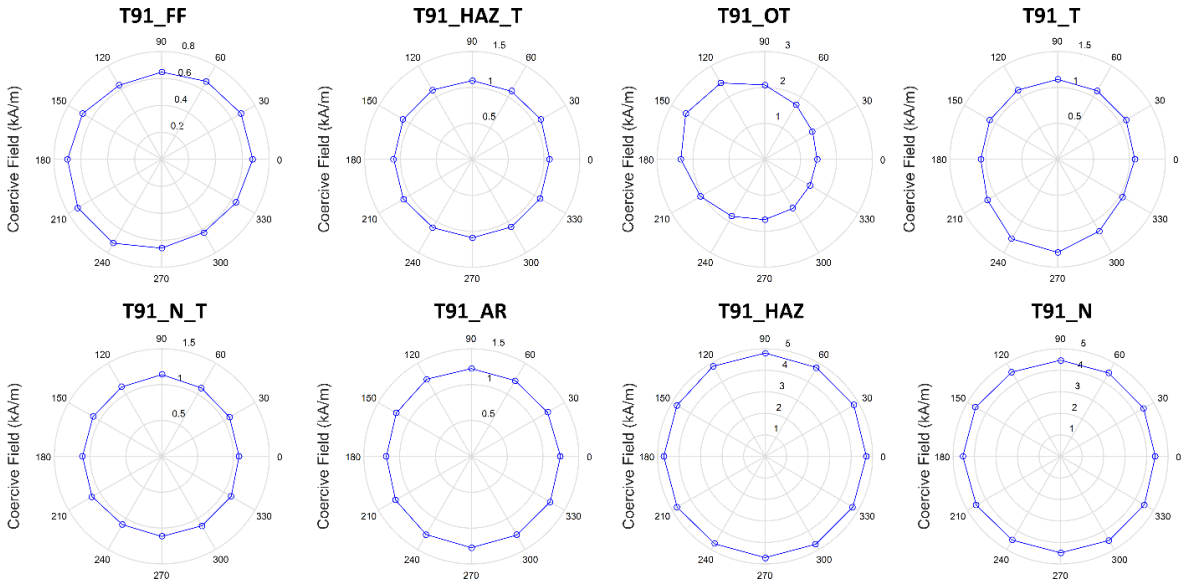

Figure 20. Polar plots of coercive field for identified tube samples

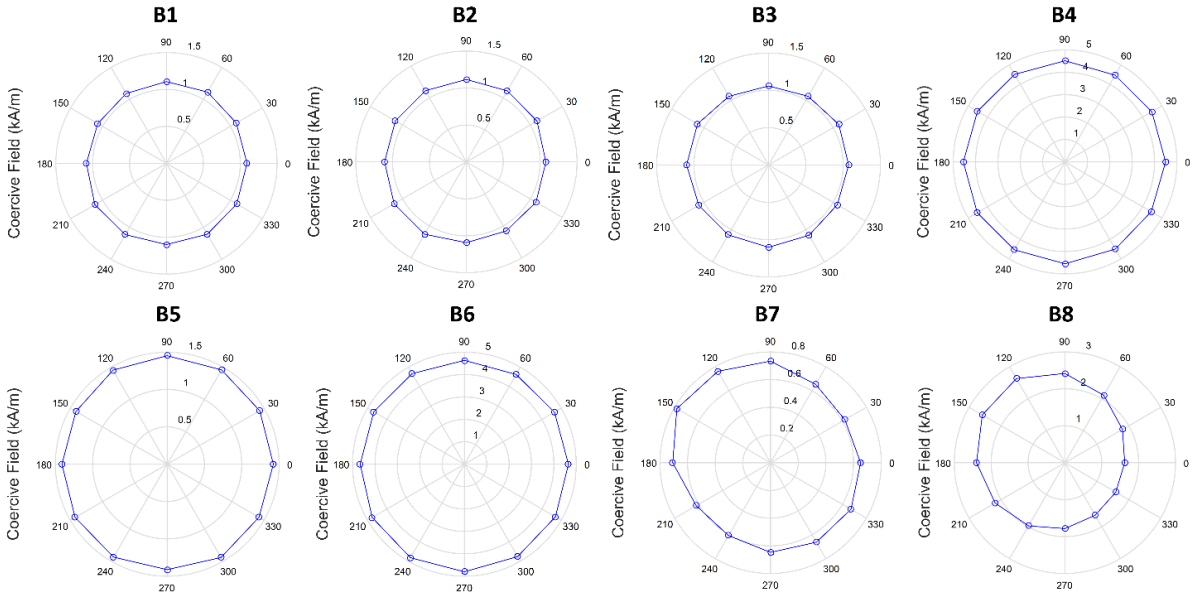

Figure 21. Polar plots of coercive field for unidentified tube samples

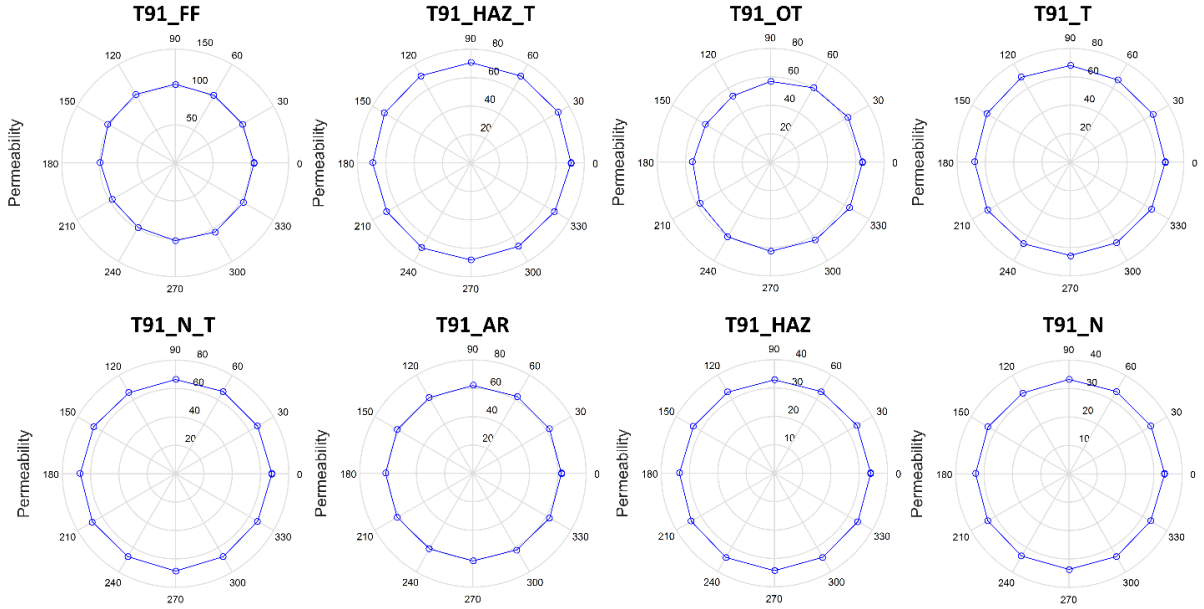

Figure 22. Polar plots of permeability for identified tube samples

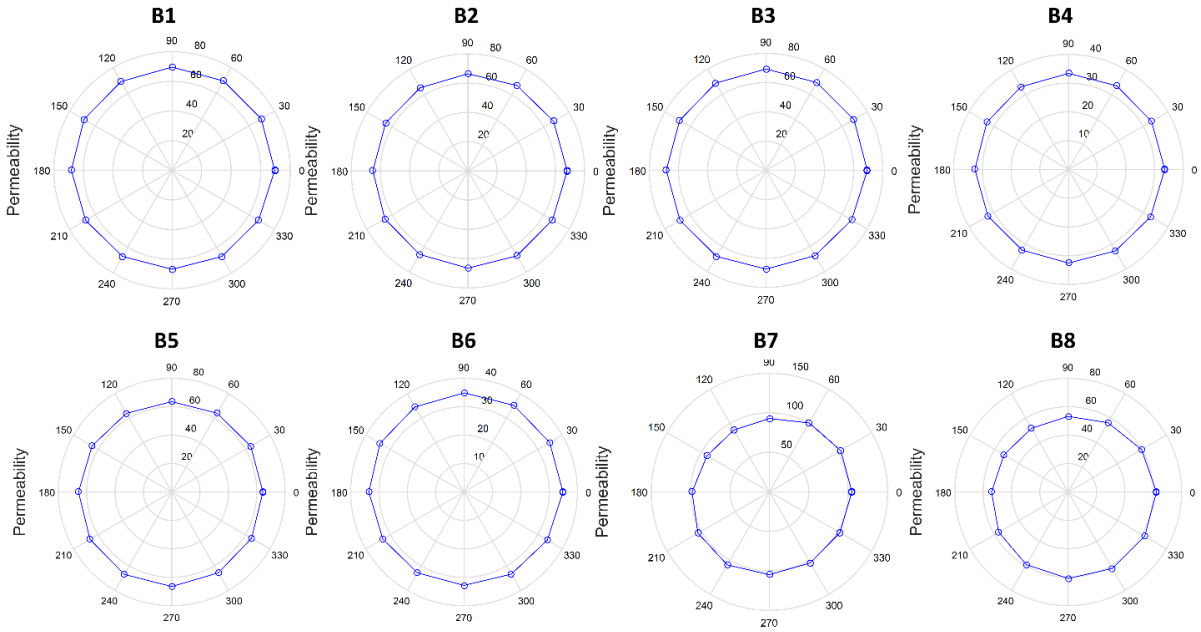

Figure 23. Polar plots of permeability for unidentified tube samples

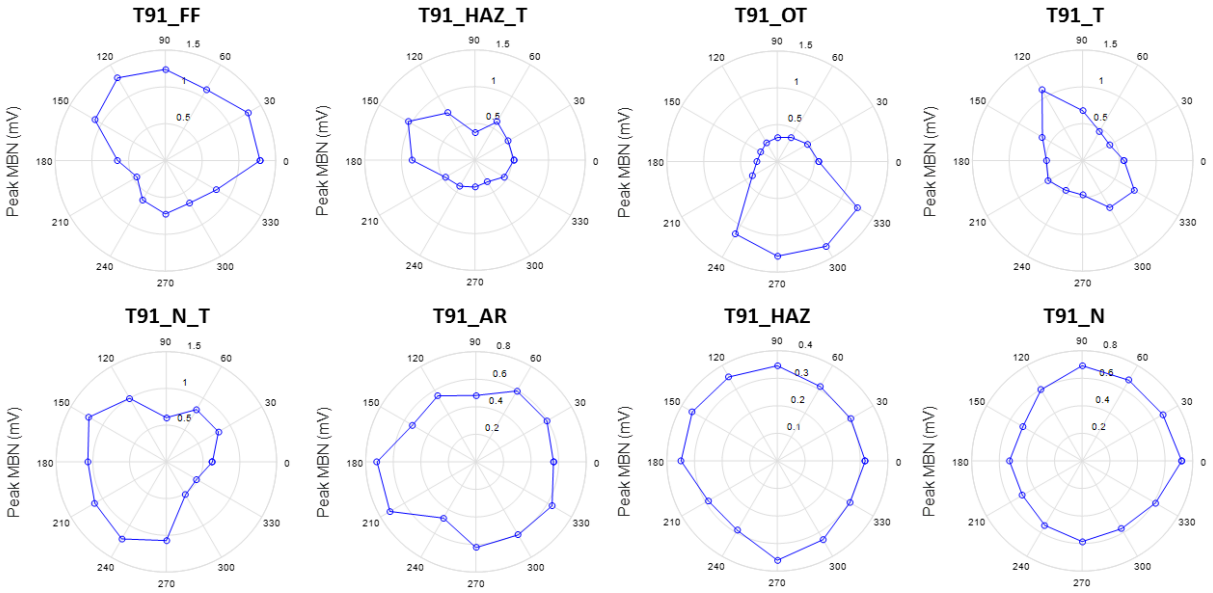

Figure 24. Polar plots of peak MBN for identified tube samples

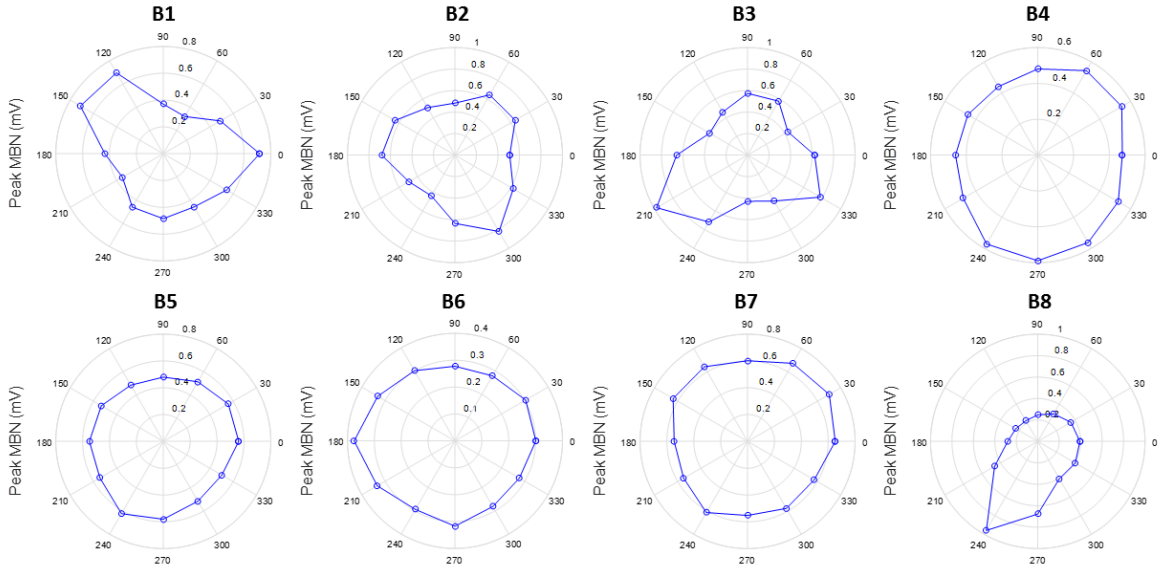

Figure 25. Polar plots of peak MBN for unidentified tube samples